



Numerical and experimental characterization of 3-phase rectification of nanobead dielectrophoretic transport exploiting Brownian motion

Ersin Altintas^{a,*}, Edin Sarajlic^a, Karl F. Böhringer^b, Hiroyuki Fujita^a

^a The University of Tokyo, Institute of Industrial Science, 4-6-1 Komaba Meguro, Tokyo 153-8505, Japan

^b The University of Washington, Box 352500, 234 EE/CSE Building, Seattle, WA 98195-2500, USA

ARTICLE INFO

Article history:

Received 8 December 2008

Received in revised form 10 May 2009

Accepted 29 May 2009

Available online 18 June 2009

Keywords:

Brownian motion

Brownian motor

Microchannel

Nanobeads

Net-unidirectional motion

Numerical analysis

PDMS

Ratchet

ABSTRACT

We report on a transport system for nanobeads that exploits Brownian motion as the main actuation source, saving energy compared to a purely electrostatic transport system of the same geometry. The transport system employs a microfluidic channel to restrict Brownian motion of the nanobeads to only one dimension and a 3-phase dielectrophoretic flashing ratchet to bias the spatial probability distribution into the rectification direction for one-dimensional transport. A numerical model of the system is developed and applied to investigate its performance. A micromachined transport system is fabricated and employed to experimentally validate the model with the confirmation of the optimal operation point. Numerical model and experiments have shown good agreement.

Crown Copyright © 2009 Published by Elsevier B.V. All rights reserved.

1. Introduction

Microsystems for transportation of small objects were demonstrated using conventional actuation methods such as electrostatic comb-drive actuators [1], thermally actuated ciliary motion of arrayed bimorph cantilevers [2], distributed pneumatic actuators [3], and acoustic waves [4]. However, in general, by reducing the size of objects being transported down to micro- and nanoscales, physical and/or chemical phenomena negligible at macro-scales can come into action and even be employed for the actuation. For instance, recently, surface tension has been introduced for the actuation of microstructures [5], and catalytic reactions have been employed for rotation of nanorods made of Au and Pt [6], and cargo carrying [7].

Brownian motion, caused by thermal fluctuations in liquids [8–10], is one of the dominating phenomena at nanoscale, and therefore a promising candidate for actuation of nano-objects. Bio-molecular motors have evolved to exploit this thermal phenomenon in the realm of low Reynolds number where inertial forces are overwhelmed by viscous forces that damp any motion [10–12]. For nanosystems operating in liquid, therefore, it would be preferable to accommodate the effects of Brownian motion sim-

ilar to bio-molecular motors. However, due to the stochastic nature of Brownian motion [9,12–16], a defined motion is not achievable unless external energy is introduced into the system [14]. In this sense, flashing ratchets or Brownian motors are good examples how to rectify the random thermal motion [9,14–16].

In this paper, we introduce an alternative nano-transport system of nanoparticles (nanobeads) based on Brownian motion, i.e. a linear Brownian motor (LBM), inspired by bio-molecular motors. LBM employs microchannels to restrict the random motion of nanobeads into one dimension in a similar fashion as microtubules and actin filaments guide kinesin and myosin, respectively (Fig. 1a) [10,12]. The net-unidirectional or directed motion of nanobeads is achieved using 3-phase dielectrophoretic rectification to bias their spatial probability distribution as illustrated in Fig. 1b. In this way, the probability of a nanobead moving in rectification direction becomes higher than the probability of that nanobead moving in the opposite direction. This approach is different from Brownian motors based on asymmetric and periodic potentials, where electrical force is directly responsible to move the particles to potential minima [15,16]. In our system, the electrostatic trapping force used for rectification is kept small enough to prevent attraction of the nanobead directly from the adjacent inactive electrodes (grounded) which gives rise to an electrically actuated transport (i.e. electrostatic actuation region). On the other hand, the force must be sufficient to counteract the Brownian force on the active electrode (voltage applied) to overcome random effects of the motion. This implies the

* Corresponding author. Tel.: +81 03 5452 6249; fax: +81 03 5452 6250.

E-mail addresses: e-altintas@bk.jp.nec.com, ersin@iis.u-tokyo.ac.jp (E. Altintas).

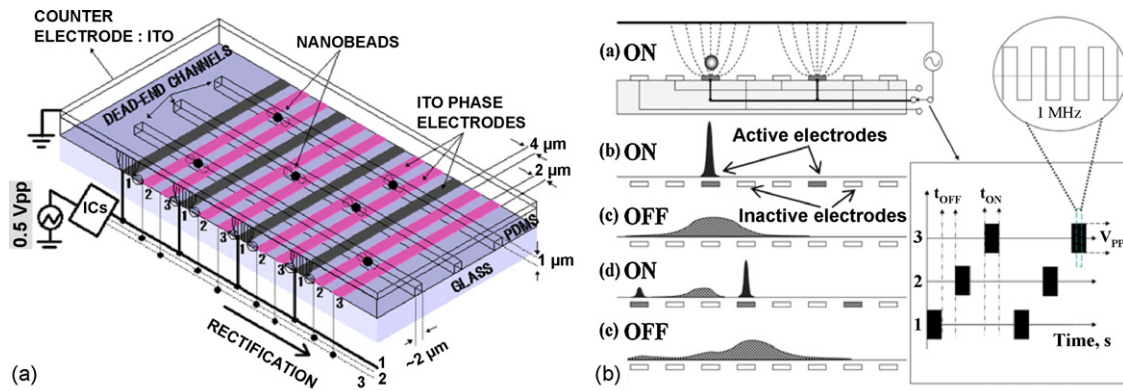


Fig. 1. (a) Schematic of micromachined linear Brownian motor (LBM). Patterned PDMS sheet on a glass substrate provides microchannels. 3D Brownian motion is restricted in the microchannel and turned into 1D motion. ITO line electrodes of $2\ \mu\text{m}$ width and $4\ \mu\text{m}$ spacing (LBM-4) are made on the glass substrate. The channels and the electrode are placed orthogonally to each other. 3-Phase electrostatic field rectifies this random motion. (E-field is shown on the left side only. Device is not to scale.) (b) Transportation by 3-phase DEP (flashing) ratchet and biasing the spatial probability distribution of a nanobead.

existence of three different regions of operation; (i) electrostatic region, (ii) Brownian motor region and (iii) Brownian motion (random) region. In the Brownian motor region, Brownian motion is the dominant source of actuation to transport nanoparticles between electrodes, and electrostatic force is the rectifier. Consequently, the driving voltage and the energy consumption in LBM that exploits Brownian motion for the transportation of the nanoparticle are lower compared to the same system that uses the pure electrical transportation.

Previously, we have proved the feasibility of the LBM and shown its performance as a function of applied voltage. Furthermore, we have shown that the effects of alternative current (AC) electro-osmotic and thermal flows on the motor performance were negligible [17,18]. In this paper, we develop a numerical model and use it to further investigate the performance of the system as function of different design and actuation parameters, such as size applied voltage and switching time. In addition, we have fabricated an improved LBM with increased number of electrodes and employed it to experimentally validate the theoretical model. The optimal transport region of LBM is investigated both theoretically and experimentally.

2. Numerical model

The device was modeled by finite element methods in COMSOL Multiphysics™ (formerly FEMLAB).

The model consists of a microchannel with three integrated electrodes buried into the glass substrate (Fig. 2). The microchannel, which is $1000\ \text{nm}$ high, is filled with deionized water (DIW). The upper part of the channel is PDMS, while the lower part, in which electrodes are located, is oxide dopant coating (OCD) deposited on the glass. The diameter of the transported nanobead was set to $500\ \text{nm}$. Electrical potentials of the electrodes were defined at the electrode circumference. Relative permittivity of DIW at the temperatures of 20 and $25\ ^\circ\text{C}$ is 80 and 78.3 , respectively. In our numerical simulations, we assumed the relative permittivity of 80 ignoring the 2% difference. Furthermore, we assumed that dilution of nanobeads with DIW and the applied frequency do not have any influence on the properties of the DIW.

Dielectrophoresis (DEP) is the induced motion of polarizable particles in a non-uniform electrical field. Time averaged DEP force on a spherical particle is dependent on the volume of the particle of radius a , the permittivity of the medium (ϵ_m), the real part of the polarization factor (Clausius–Mossotti factor, f_{CM}) and the gradient of electrical field squared, which is given by

$$\langle F_{DEP} \rangle = 2\pi a^3 \epsilon_m \text{Re}\{f_{CM}\} \nabla |E_{rms}|^2 \quad (1)$$

The properties of the particle, medium and the applied frequency change the polarization factor, which ranges between -0.5 and 1.0 for a spherical particle (or a nanobead). This factor determines the nature of DEP; positive or negative (attractive or repulsive), respectively. The exact determination of this factor is difficult. In our previous experiments we have observed that a nanobead was attracted to the active electrode at $1\ \text{MHz}$, showing that the factor is positive. In the simulations we assumed that it is 1 for simplicity of calculation, as commonly done [19,20].

In our 3-phase numerical system, the active electrode is set to a certain voltage and other two inactive electrodes are electrically grounded. The magnitude and behavior of DEP force at the center of the channel was investigated. Based on these analyses, the DEP force was calculated to be the highest at the center of the active electrode and changing its direction towards the electrode edges. A particle located in the vicinity of the active electrode is attracted towards the center. This modeled DEP force decreased in an inversely cubic manner with the distance, due to the assumption of semi-circular electric field lines between electrodes [20]. The simplified model was defined to follow the field distribution obtained by the finite element on and around the active electrode (Fig. 3). Brownian

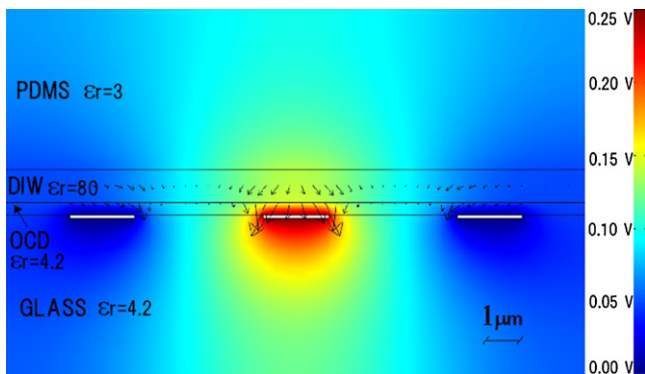


Fig. 2. (color online) Cross-section of modeled device by finite element methods (Comsol). The device is composed of glass ($\epsilon_r = 4.2$), oxide dopant coating (OCD, $\epsilon_r = 4.2$), microchannel with DIW ($\epsilon_r = 80$) and PDMS ($\epsilon_r = 3$). The thickness of glass and PDMS is set to $5\ \mu\text{m}$ due to resolution limits. Color represents the electrical potential, and arrows directing towards electrodes represent dielectrophoretic (DEP) force. $0.25\ \text{V}$ is applied to the electrode at the center and the others are grounded. The diameter of the particle and the temperature is $500\ \text{nm}$ and $25\ ^\circ\text{C}$, respectively. Continuity equations at the internal boundaries between interfaces are provided and any surface charges and polarizations at the interfaces are ignored. The outer boundary conditions are set to zero-charge symmetry. The mesh size at the channel is $50\ \text{nm}$, while it is $200\ \text{nm}$ out of the microchannel region due to memory problems.

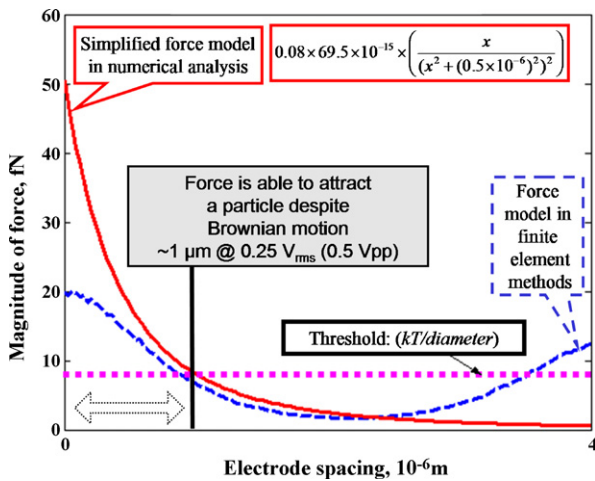


Fig. 3. Comparison of forces at the center of PDMS microchannel. Threshold force in magnitude is calculated dividing thermal energy by the diameter of the particle. Active and inactive electrode is on the left and right, respectively. Force can reach to inactive electrode due to increase in radius of a nanobead or applied voltage or decrease in electrode spacing (DEP force), which causes a purely electrical transport.

motion of nanobeads was modeled by random numbers with normal distribution. Standard deviation was adjusted by the diffusion constant of the nanobeads used in the experiments. The nanobead motion was simulated in one direction only. The threshold force of the system was calculated as follows. Each segment of random motion was assumed in the order of the diameter of the nanobead. The particle had the same thermal energy as the surrounding liquid molecules. This energy should be equal to the work done by Brownian force acting over a distance equal to the diameter [17,21].

Different parameters, related to DEP force or Brownian motion, influence the performance of the system. We have evaluated the performance of the system as a function of the size of the particle, applied voltage, electrode spacing, viscosity and temperature, switching ON/OFF time. Here, we will mention about the influence of applied voltage and timing only.

2.1. Influence of applied voltage

The DEP force is related to the square of the voltage applied [19,20]. In our first paper, we have shown that increased voltage causes more shifts of the distribution of the nanobeads to the rectification direction [17]. This implies that increasing voltage give rise to an electrostatic actuation and an increasing average speed. We can differentiate 3 different regions (Fig. 4a). Above 0.95 V_{rms}, the force is able to attract the particle from adjacent inactive electrodes despite Brownian motion, which gives rise to an electrostatic actuation region. Below 0.075 V_{rms}, no net motion is observed and LBM cannot provide control over Brownian motion, which leads to a Brownian motion region. In the window region between 0.075 and 0.95 V_{rms}, transportation of nanobeads is partially achieved by Brownian motion and DEP rectification (Brownian motor region). The average speed in the Brownian motor region is less than that of the electrostatic region. The average speed increases with the applied voltage because of the increase in the rectification force, which implies increase in the energy consumption.

2.2. Influence of switching time

The switching sequence, illustrated in Fig. 1b, is one of the most important parameters of the Brownian motor. In our configuration, electrodes of one phase are activated at a time. After the activation period (ON time, *t*_{ON}), the voltage is switched off (OFF time, *t*_{OFF}) before the electrodes of the next phase are activated. The diameter of our particle is 500 nm. In DIW at room temperature, diffusion distance in 1 s is 1 μm in rms and comparable to the width and separation of electrodes. Therefore, the unit of *t*_{OFF} and *t*_{ON} must be set to seconds rather than milliseconds or minutes. Simulated performance of our motor for different switching sequences is shown in Fig. 4b. At low regimes of *t*_{ON} below 4 s, the speed performance is strongly dependent on *t*_{OFF}. With increasing *t*_{OFF}, it increases to peaks around 4.5 ± 0.5 s and then decreases. *t*_{OFF} is comparable to the expected diffusion time of particles between electrodes (8 s). As we increase *t*_{ON}, the peak point shifts to the shorter *t*_{OFF}; this shows the importance of *t*_{ON} in the speed performance. When *t*_{ON} is more than 8 s, the influence of *t*_{ON} dominates over *t*_{OFF}. The system reaches its optimal performance, which is around 63 nm/s, when *t*_{OFF} and *t*_{ON} are 0 and 16 s, respectively. However, further

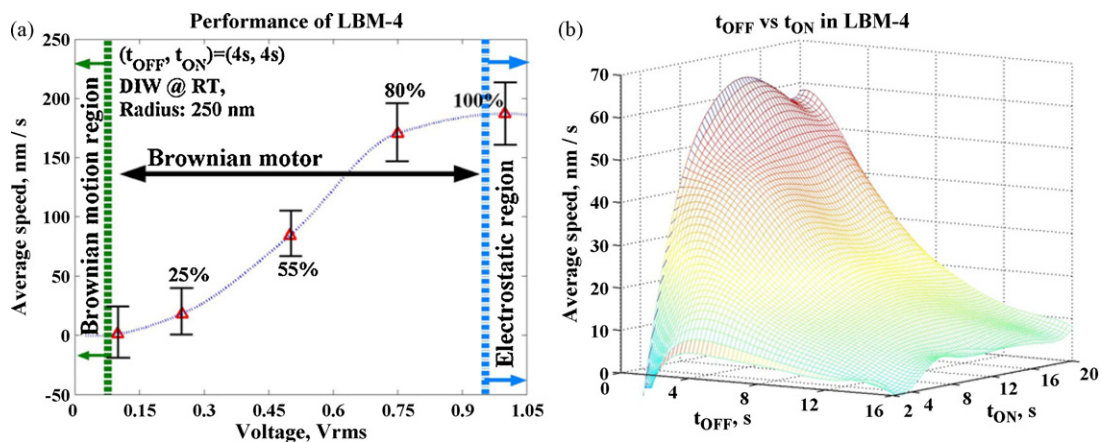


Fig. 4. (color online) Simulated speed performance of LBM-4 with respect to different parameters. All curves are fitting. (a) Influence of the applied voltage. It changes the mode of operation. The window is Brownian motor region where Brownian motion is the source of actuation and DEP force is the rectifier. Values in % represent the effective range of electric force to attract a particle despite Brownian motion; 100% correspond to the full electrode spacing. (b) Influences of OFF and ON time. At low regimes of ON time, OFF time causes curves to peak at a value comparable to the expected diffusion time of nanobeads (i.e. 8 s). As ON time increases, peaks shift to shorter OFF time and ON time starts to dominate over the speed performance. The optimal speed is around 63 nm/s and attained when ON and OFF time is set to 16 and 0 s, respectively. (Applied voltage is 0.25 V_{rms}, radius of the nanobead is 250 nm, permittivity of the medium is 80 × 8.854 × 10⁻¹² F/m, temperature is 25 °C, viscosity is 0.89 × 10⁻³ Pa s, time resolution is 5 ms, and undersampling is 100, respectively.)

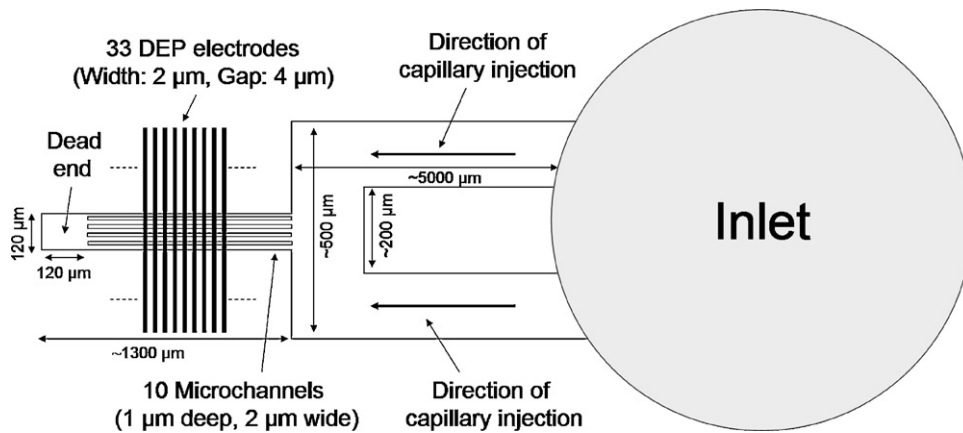


Fig. 5. Schematic top view of the device with the alignment of the PDMS and 3-phase ITO electrodes. Total number of electrodes is 33. Introduction of nanobeads is achieved by capillary forces due to the hydrophilic channel walls.

increase of t_{ON} will not improve the performance of the system, since nanobeads stay on active electrodes for too long.

2.3. Theoretical investigation of optimal switching

To theoretically investigate the optimal switching timing of the system, we assumed two active electrodes that are infinitely narrow. These active electrodes serve as the absorbers of nanobeads. Two other electrodes located between these active electrodes are electrically grounded and are not capable of attracting the nanobeads. The mean time to capture a nanobead between the active electrodes can be given by

$$\frac{bx - x^2}{2D} \quad (2)$$

where b , x , D are the spacing between two active electrodes, position of the nanobead and the diffusion constant of the particle, respectively [22]. From this equation, it follows that the optimal performance of the motor is strongly dependent on the electrode spacing, electrode width and diffusion constant (i.e. proportional to the absolute temperature and inversely proportional to the size of the particle and the viscosity of the medium). By increasing electrode width implies an additional distance for particles to diffuse,

increasing the optimal capture time. If we consider a 3-phase configuration with an electrode width of $2 \mu\text{m}$, then b will be equal to $14 \mu\text{m}$ due to the ability of the force to attract a nanobead $1 \mu\text{m}$ away from the active electrode (Fig. 3). The average of mean time to capture a particle anywhere between active electrodes will be $b^2/2D$, which is equal to 16.5 s for our system. This value is consistent with the simulations.

3. Device fabrication

Our experimental device, schematically shown in Fig. 5, consists of a glass substrate (Matsunami, $150 \mu\text{m}$, $24 \text{ mm} \times 36 \text{ mm}$) with indium tin oxide (ITO) electrodes covered by a poly(dimethylsiloxane) (PDMS) sheet with microchannels aligned to the electrodes. The flow of the fabrication process is shown in Fig. 6. For the electrode fabrication, we used a lift-off process. First, a S1818 photoresist (Shipley) of $2 \mu\text{m}$ thickness was patterned on the glass (Fig. 6a). After the postbake of the photoresist (Fig. 6b), the glass was isotropically etched in a buffered hydrofluoric acid (BHF, 1%) for 30 s to a depth of 100 nm in order to facilitate the lift-off process (Fig. 6c). After etching, a 100 nm thick ITO layer was sputter-deposited to form electrodes (Fig. 6d). Consequently, a 100 nm thick Cr–Au layer was deposited to define the wire bonding

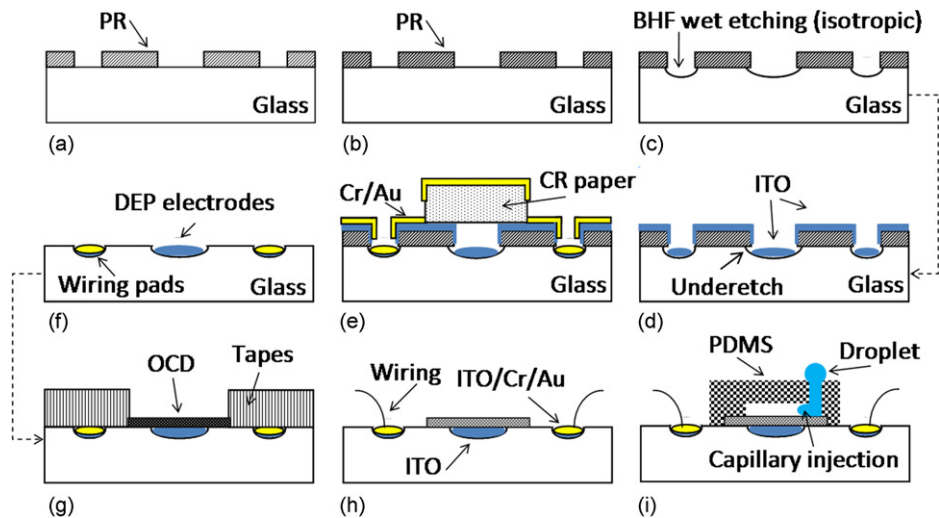


Fig. 6. The flow of the fabrication of the device. (a) Patterning of photoresist, (b) Hardbake of the photoresist, (c) Isotropic etching of the glass substrate by BHF, (d) ITO sputtering, (e) shadow masking at electrode region by clean room (CR) paper and Cr–Au sputtering, (f) removal of CR paper and lift-off process, (g) protection of wiring pads by CR tape and OCD coating, (h) Hardbake of OCD and wiring, (i) Manual alignment of PDMS and injection of nanobead suspension by capillary forces. (Images are not to the scale and they do not correspond to the real cross-section of the device.)

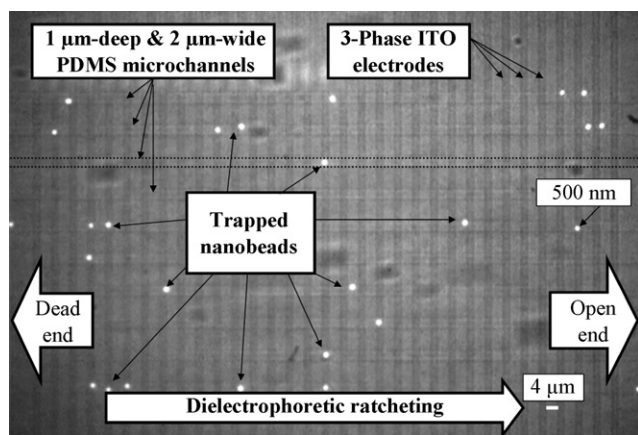


Fig. 7. Optical micrograph during experiment with LBM-4. Nanobeads are trapped in the channels and they experience Brownian motion (OFF state). Orthogonal alignment of ITO electrodes with PDMS microchannels was achieved manually, and misalignments were measured less than 2° . The monitor is able to show the whole rectification area, and the nanobeads can be traced for a distance of $200\ \mu\text{m}$.

pads. Electrode region was protected by a shadow mask (Fig. 6e). Following the metal deposition, a lift-off process was performed by dissolving the photoresist with acetone in an ultrasonic bath (Fig. 6f). The sample was annealed at 300°C for 5 h to increase the conductivity of ITO electrodes. By protecting the pads with a masking tape, a hydrophilic insulation layer (Oxide Coating Dopant, OCD, 12000-T) of expected thickness around $400\ \text{nm}$ was spin-coated for a smooth surface and baked. Finally, wire bonding was conducted (Fig. 6gh).

On the other hand, PDMS microchannels were prepared from a silicon (Si) mold. A Si substrate was cleaned first and then spin-coated by the S1818 photoresist. After patterning of the photoresist, Si was etched to $1\ \mu\text{m}$ depth in a deep reactive ion etching system (Surface Technology Systems, STS, MultiPlex ASE, ST3644). After removal of the photoresist, the surface of the substrate was modified by CHF_3 plasma [23], in a reactive ion etching system (Samco, RIE-10NR) to enhance the removal of PDMS from the mold [24]. PDMS mixture was then prepared from silicone elastomer, curing agent and FZ-77, respectively (50:50:1, in weight, Dow Corning). PDMS was hydrophobic; hence we included FZ-77 to in order to make PDMS hydrophilic, allowing it to carry the nanobead suspension with the help of capillary forces. After mixing and degassing, PDMS was poured onto the Si mold, and spin-coated at 300 rpm for 60 s followed by 3000 rpm for 2 s. Next, the sample was cured at 110°C on a hot plate for 1 h. The thickness of the PDMS sheet above the channels was measured around $100\ \mu\text{m}$. Subsequently, PDMS was peeled off gently, and an inlet was punched and opened. Finally, the PDMS sheet was aligned and bonded with the glass substrate to form the microchannels (Fig. 6i). The microchannels were aligned manually to the electrodes and misalignments were measured at less than 2° (Fig. 7). The microchannels were $2\ \mu\text{m}$ wide and $1\ \mu\text{m}$ deep. The cross-section of the channel is slightly larger than the diameter of the nanobeads ($500\ \text{nm}$), allowing successful constrained motion into 1D [17,25].

In our device we have carefully chosen dimensions of the microchannels ($1\ \mu\text{m}$ in depth) and the size of the nanobeads ($500\ \text{nm}$ in diameter) in order to facilitate its fabrication and to allow simple and reliable observation of the nanobeads during the experiments. In general, particles with smaller diameter ($\sim 100\ \text{nm}$) will obviously experiences larger Brownian motion and accordingly diffuse faster. However, fabrication of the microchannels with dimensions comparable with this particle size is not trivial. Due to the low Young's modulus of PDMS, channels with a small depth can easily collapse and adhere to the surface of the glass substrate.

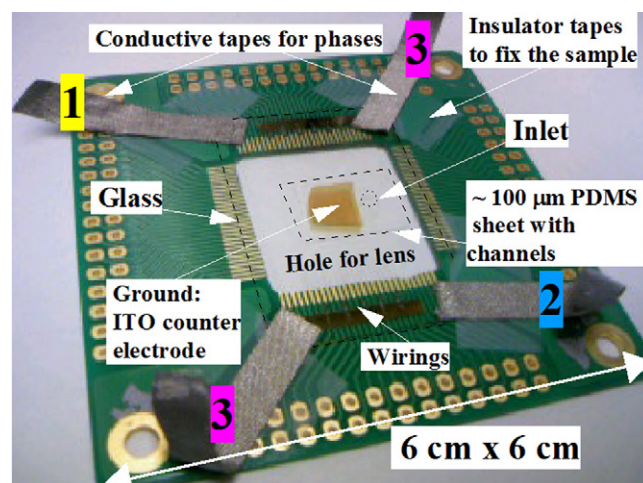


Fig. 8. Fabricated device used in the experiment. LBM-4 is fixed on a pinch board with a hole at the center for the objective lens of the microscope.

On the other hand, by employing small nanobeads in relatively large microchannels both control and rectification of their motion become rather difficult. Furthermore, the optical microscope, used for the monitoring of the nanobeads motion, imposes a resolution limit making the observation of smaller nanobeads in a larger area more challenging. In our design with dimensions mentioned above, both fabrication and observation were possible. In our experiments, we fixed the objective lens of the microscope on the overlapped area of 33 ITO electrodes and 10 microchannels (Figs. 5 and 7). In this way, we were able to observe the whole region where rectification was performed.

4. Experiments and discussions

Experimental observations were performed with an inverted microscope (Olympus IX71). The aligned sample was fixed onto a pinch board whose center had a hole for the objective of the microscope (Fig. 8). The sample was fixed onto the stage of the microscope to prevent any external vibrations or mechanical stimuli. Electrical connections were provided by a conductive tape. The 3-phase switching was achieved using an IC circuit. We used a video recording system to capture and analyze the experimental results (Sony DVD recorder, RDR-HX10). The motion of the nanobeads was recorded with a speed of 30 frames/s. Diluted suspension of fluorescent nanobeads (Fluoresbrite plain microspheres, $1.06\ \text{g}/\text{cm}^3$, 2.5% solid latex, $0.5\ \mu\text{m}$, Yellow-Green, Polysciences Inc., 1 (original):1000 (DIW)) was injected into the inlet. After the solution reached the microchannels by capillary forces due to hydrophilic walls of PDMS and the OCD layer on ITO electrodes, it was left untouched until stabilization was achieved. During the injection, it was observed that air leaked out either through the inlet and/or PDMS, which was gas permeable [26,27]. Next, the counter ITO electrode with good conductance was placed on the PDMS sheet. This electrode consists of the cover glass whose both sides were sputter-coated by ITO. The counter electrode were electrically grounded using a mechanical probe. The applied voltage between active electrodes and the counter electrode is set to $0.25\ V_{\text{rms}}$ at 1 MHz. The high frequency signal is used to prevent an undesirable liquid flow created at low frequencies due to the AC electro-osmosis [17,20,21]. In addition, nanobeads dispersed in DIW could have net electrical charges on them and therefore they can experience electrophoresis. Due to the high frequency of 1 MHz, the displacement caused by electrophoresis will be negligible [20]. By further increasing the driving frequency (limit of our function generator was 10 MHz) could possibly change the direction of DEP force; i.e.

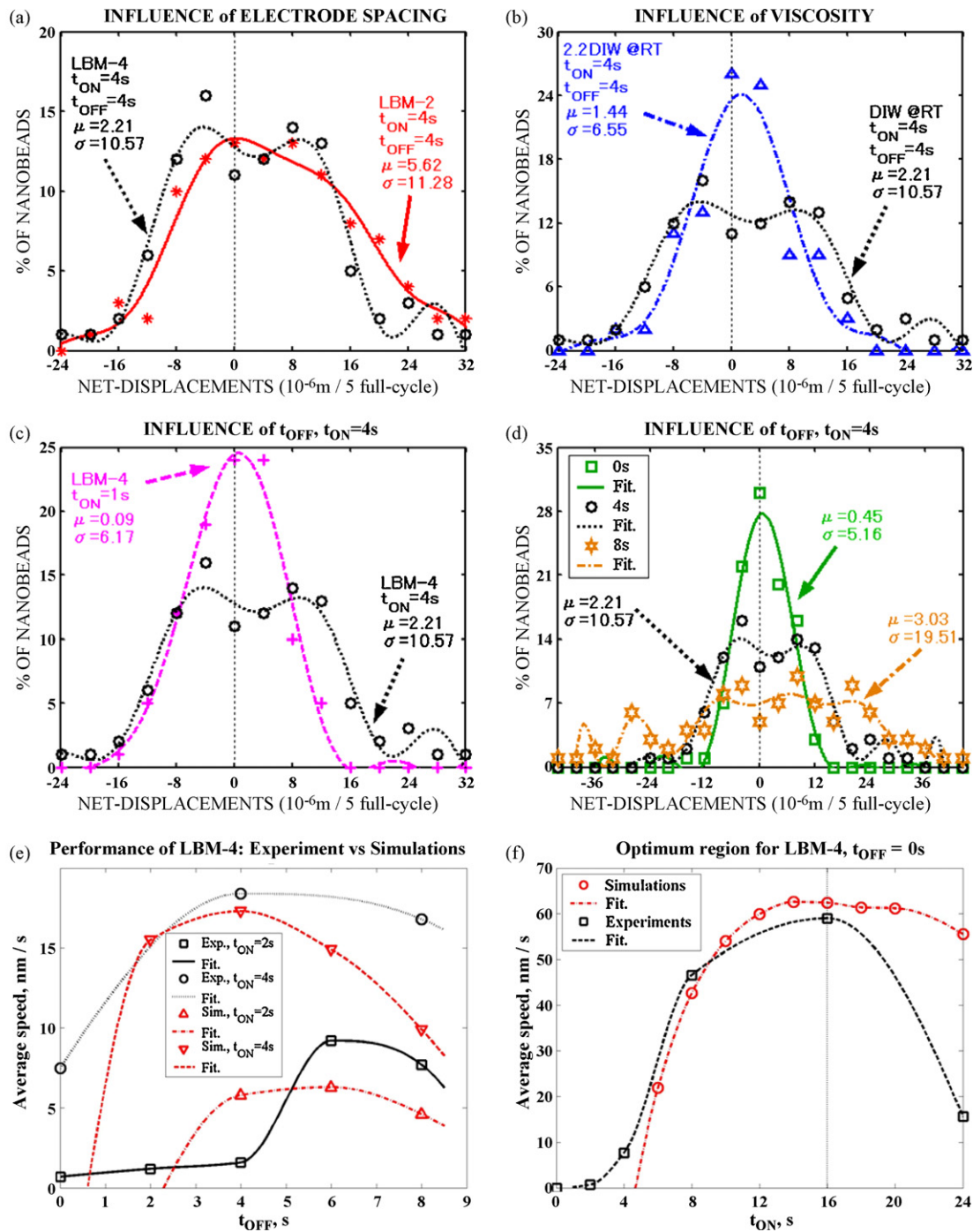


Fig. 9. Experimental characterization of LBM-4 with different parameters at room temperature with $0.25 V_{rms}$ of applied voltage at 1 MHz. Rectification is to the right. μ and σ stand for the mean and the standard deviation of the distribution, respectively. All curves are fitting. (a) Influence of electrode spacing. Decreasing spacing from 4 (LBM-4) to 2 μm (LBM-2) increases the average of the net-displacements of transports 154%. (b) Influence of viscosity of the medium. Increasing viscosity 2.2 times of that of DIW at room temperature by mixing triton-X-100 decreases the average of the net-displacements of transports 35%. (c) Influence of ON time. Keeping OFF time at 4 s, and decreasing ON time from 4 to 1 s, decreases the average of the net-displacements of transports 96%. (d) Influence of OFF time. As OFF time increases, the distribution spreads more and deviations become larger. (e) Influences of ON and OFF time and comparisons of both simulations and experiments. Both peak at similar regions, and then speed performance decreases with increasing OFF time. Peaks are comparable to the expected diffusion time of nanobeads between electrodes (i.e. 8 s). (f) Optimal region in LBM-4. The optimal speed is around 60 nm/s and attained when ON time and OFF time is set to 16 and 0 s, respectively. Simulations and experiments are in good agreement.

negative DEP. In our previous experiments [17], we had observed that 1 MHz was sufficient to eliminate AC electro-osmosis and the particles were attracted to the electrodes on which voltage was applied.

We have experimentally investigated performance of the LBM as function of different parameters: electrode spacing, viscosity, t_{ON} , and t_{OFF} , when $0.25 V_{rms}$ was applied (Fig. 9a–d). The device with

4 μm spacing between the electrodes was the reference device and named LBM-4. We have worked with a large number of particles (around 100) to investigate their net-displacements (Table 1). Displacement videos were divided into 5 full-cycles for distribution analysis only (e.g. $5 \times 3 \times (t_{ON} + t_{OFF})$). Except otherwise stated, t_{ON} and t_{OFF} were set to 4 s. The distance from the initial to the final position of the nanobeads (net-displacement) was determined in the

Table 1
Experimental data and reported values with switching time and traced number of nanobeads. Data show the displacement of the distribution of traced nanobeads over the course of time before and after the experiment with respect to switching time. In the last row, data related to viscosity experiment are provided as well. We reported the A–B value with the assumption that the bias before the experiments did not change its speed during the experiments. Data when A was smaller than B ($A - B < 0$) were discarded. We do not have any test before experiments in LBM-2 only, (Ref and Opt stand for reference device and optimum point, respectively).

(t_{ON}, t_{OFF}) (s, s)	Displacement before voltage application (Ave., μm) (B)	Displacement after voltage application (Ave., μm) (A)	Standard deviation (μm) (σ)	Reported displacement value (μm) (A – B)	Experimental time interval (s) (Δt)	Average speed (nm/s) $((A - B)/\Delta t)$	Number of nanobeads
(4,4)	1.45	3.66 (Ref.)	10.57	2.21	120	18.4	127
(16,0)	-3.81	-0.98 (Opt.)	5.46	2.83	48	59	40
(24,0)	3.67	4.97	6.85	1.12	72	15.6	91
(8,0)	-9.05	-3.47	12.2	5.59	120	46.6	192
(4,8)	-2.21	0.81	19.51	3.03	180	16.8	147
(4,0)	11.95	12.39	5.16	0.45	60	7.5	123
(2,8)	3.43	4.58	7.6	1.15	150	7.7	37
(2,6)	5.04	6.13	9.85	1.1	120	9.2	146
(2,4)	1.7	1.85	7.56	0.14	90	1.6	87
(2,2)	7.25	7.32	6.47	0.07	60	1.2	91
(2,0)	-0.05	-0.03	5.34	0.02	30	0.7	160
(1,4)	3.82	3.91	6.17	0.09	75	1.2	149
Vis. (4, 4)	29.98	31.42	6.55	1.44	120	12	141

electrode region only (i.e. the region between the 1st and the 33rd electrode). The displacement was measured in Adobe Premiere with the help of an electronic ruler (Monosashisya) and rounded to the nearest multiples of 4. During the observation, nanobeads escaping from the electrode region or stopping in the channels were not included in the measurements result. Before the experiments, a test was performed to determine a possible bias on the motion of the nanobeads. We believe that this biased motion could be induced by the inlet and the mechanical pressure caused by the grounding probe placed on the PDMS sheet. Experimental values were compensated accordingly and average value and standard deviation were calculated for each distribution (Table 1). When calculating the distribution of the average speed, we assumed that the bias measured before the experiments did not change in the course of experiments. Furthermore, when the net displacement with voltage application was smaller than the net displacement without voltage application, data were discarded.

4.1. Influence of electrode spacing on distribution

We have designed two types of device whose electrode spacings were 2 and 4 μm [28], respectively (Fig. 9a). For both devices, distributions of the nanobeads were shifted to the rectification direction, i.e. to the right. In LBM-2, 59% of the nanobeads were transported in positive direction (28% in negative, 13% no net-displacement) whereas it was 51% in LBM-4 (38% in negative, 11% no net-displacement). These results revealed that these were not random motions, but rather slightly rectified motions. The distribution was shifted more in LBM-2. As the spacing of electrode in LBM-2 was the half of that in LBM-4, we increased the electric force 8 times at a constant voltage and decreased the diffusion length of the particles. In this way, transports in LBM-2 were partially achieved by electrical attractions. These modifications increased net displacements of the nanobeads and caused a larger average displacement in LBM-2 (5.62 μm) compared to LBM-4 (2.21 μm) such that average of the distribution increased 154%.

4.2. Influence of viscosity on distribution

The next parameter that we investigated was the viscosity of the fluid (Fig. 9b). We mixed triton-X-100 with DIW (10% vs. 90% in weight) to reach a viscosity of 2×10^{-3} Pa s at room temperature. The viscosity of the solution was almost 2.2 times of DIW at room temperature. Although the same driving voltage of $0.25 V_{\text{rms}}$ was applied in both experiments, mixing DIW with triton-X-100 could change the permittivity and Clausius–Mossotti factor of the solution, resulting in a different effective force. The displacement results revealed that in more viscous medium than DIW water, the average of the displacements was decreased 35% (1.44 μm vs. 2.21 μm). Furthermore, 84% of the net-displacements were between -8 and 8 μm . In conclusion, higher viscosity caused Brownian activity to decrease and led to smaller average speed (Table 1).

4.3. Influence of ON time on distribution

Using the LBM-4 device, we have investigated the influence of the ON time, the time during which the driving voltage was applied on a certain phase, on the motor performance (Fig. 1b). In these experiments the ON time was varied while the OFF time was fixed to 4 s. As shown in Fig. 9c, the variations in the ON time have strongly affected the displacement of the nanobeads. By decreasing the ON time from 4 to 1 s, the average of the distribution decreased 96% (0.09 μm vs. 2.21 μm). During the experiments, long displacements of the nanobeads did not occur, corresponding to the 89% of the net-displacements which were between -8 and 8 μm . Actu-

ally, this was an expected result that with longer ON times it was more probable to capture and to rectify the nanobeads by active electrodes.

4.4. Influence of OFF time on distribution

Another parameter was the OFF time (Fig. 9d), the time during which no electrode was activated (Fig. 1b). To investigate the influence of the OFF time, we fixed ON time to 4 s, and changed the OFF time as 0, 4 and 8 s, respectively. As the OFF time increased, the ranges of the net-displacements were increased and so was the average of the distributions. The increase OFF time provided more distributed and dispersed nanobeads over electrodes. The increases in the standard deviations were indicators of widening as well.

4.5. Influence of OFF/ON time on speed performance

The important consideration was the characterization of the speed performance of the system in terms of OFF and ON time (Fig. 9e). The speed performance was strongly dependent on both OFF time and ON time. By comparing ON time at 4 and 2 s in Fig. 9e, it is clear that the performance increased with ON time. In a fixed ON time, the speed performance peaks around 5.5 ± 1 s of OFF time comparable to the expected diffusion time (6.2 s) of particles between electrodes [28], and then decreases if we continue to increase OFF time. This shows that even though we can get larger transports of nanobeads over electrodes, the overall average speed of the distribution will decrease, because diffusion length is proportional to the squared root of time. Experiments and simulations made peaks at similar points and then decreased, showing a good agreement.

4.6. Experiments vs. simulations and optimal speed performance

The next investigation was related to the optimal speed performance of the fabricated device. In the simulations the maximum speed at $0.25 V_{rms}$ was observed when the OFF time was zero and the ON time was 16 s (Fig. 4b). In the experiments, we set the OFF time to zero, and investigated the speed performance of the system by changing the ON time from 1 to 24 s (Fig. 9f). We have confirmed good agreements between the simulations and the experiments from 4 to 20 s. In both cases, the speed peaks around 16 s and then decreases, where (experimental) optimal average speed is 59 nm/s. The two curves do not fit very well at low (<4 s) and high (>20 s) ON time durations (Fig. 9f). This could be associated with the assumptions and estimations performed in the numerical analysis and force calculations. For example, we assumed two dominant phenomena in our system, which were DEP and Brownian motion. In the reality, there could be other phenomena that may have some influence on the speed performance of the system. In addition, another assumption was the semi-circular electric field line between coplanar electrodes, which does not match with a realistic distribution of electric field lines in reality. Those assumptions and estimations might create discrepancies at low and high ON times between numerical and experimental results. In addition to speed vs. time characteristic, the distribution in the optimal region revealed important facts (Fig. 10). We conducted the experiments with LBM-4 for 48 s corresponding to 1 full-cycle. (Long experimental times caused the nanobeads to leave the electrode area and made the analysis difficult as well.) Even though the experimental time was 48 s, the distribution of the nanobeads with ON and OFF time of 16 and 0 s, respectively, shows bigger positive shift than that with ON and OFF time of 4 and 4 s, respectively, when experimental time was 120 s (Fig. 9a, Table 1). In the optimal case, 59% of the net-displacements were in positive direction (23% in negative, 18% no net-displacement), whereas it was 51% in the non-optimal

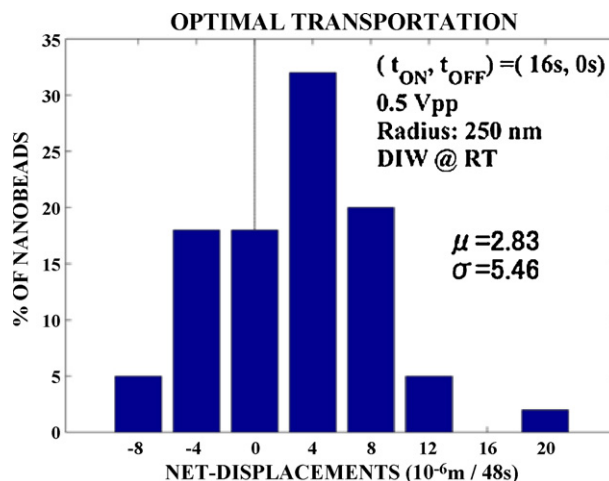


Fig. 10. Optimal transportation of LBM-4 in 48 s with ON time and OFF time of 16 and 0 s, respectively, at $0.25 V_{rms}$. 59% of particles were transported in positive direction (23% in negative).

case shown in Fig. 9a (38% in negative). The ratio of percentage of positive transports to negative transports was 2.56 and 1.34, respectively. Optimal region improved the performance in terms of speed (3 times) and the ratio of transports (2 times).

Even though we achieved biasing of the motion by 3-phase DEP forces; we observed that nanobeads could still experience Brownian motion in the close vicinity of active electrodes. These observations suggested that the force was enough to attract nanobeads despite Brownian motion in the vicinity of active electrodes and to rectify the random motion, but it was weak to immobilize the nanobead on the active electrode.

4.7. Energy saving

In our system, because of exploitation of Brownian motion, energy is saved compared to a purely electrical transport system of the same geometry, where bigger voltages are necessary to be applied (Fig. 4a). On the other hand, increasing average speed with voltage indicates an expected trade-off between energy saving and the average speed. As a result, our system is less effective in terms of positive transport of particles in a fixed time but consumes less energy.

The issue of energy saving, which is out of the scope of this paper, must be investigated in detail for better understanding of the system to use Brownian motion at nanoscales effectively and efficiently. Brownian motor exploiting Brownian motion as a driving source of actuation might lead to more energy efficient nanosystems compared to their electrically actuated counterparts.

5. Conclusions

We have exploited Brownian motion of nanobeads to achieve a directed transport of nanobeads in microfluidic channels and characterized the system in terms of several parameters. We used a micromachined 3-phase dielectrophoretic flashing ratchet to bias the spacial probability distributions of the nanobeads, rather than asymmetrical potentials. The simulations and experiments have shown net-unidirectional transport of nanobeads with good agreements in the speed performances and revealed the reduction of energy consumption. We believe that this kind of study will help nano-science and physics to understand ratcheting effects in the control or manipulation of Brownian motion.

Acknowledgements

We would like to thank to The Ministry of Education, Culture, Sports, Science and Technology, Japan, for financial support, and would like to thank to VDEC (VLSI Design and Education Center) of The University of Tokyo for the fabrication of the masks.

Appendix A. Supplementary data

Supplementary data associated with this article can be found, in the online version, at doi:10.1016/j.sna.2009.05.022.

References

- [1] P.H. Pham, D.V. Dao, S. Sugiyama, A micro transportation system (MTS) with large movement of containers driven by electrostatic comb-drive actuators, *J. Micromech. Microeng.* 17 (2007) 2125–2131.
- [2] M. Ataka, A. Omodaka, N. Takeshima, H. Fujita, Fabrication and operation of polyimide bimorph actuators for a ciliary motion system, *JMEMS* 2 (1993) 146–150.
- [3] Y. Fukuta, Y.A. Chapuis, Y. Mita, H. Fujita, Design, fabrication, and control of MEMS-based actuator arrays for air-flow distributed micromanipulation, *JMEMS* 15 (2006) 912–926.
- [4] A. Wixforth, C. Strobl, C. Gauer, A. Toegl, J. Scriba, Z.V. Guttenberg, Acoustic manipulation of small droplets, *Anal. Bioanal. Chem.* 379 (2004) 982–991.
- [5] J. Lee, C.J. Kim, Surface-tension-driven microactuation based on continuous electrowetting, *JMEMS* 9 (2000) 171–180.
- [6] L. Qin, M.J. Banholzer, X. Xu, L. Huang, C.A. Mirkin, Rational design and synthesis of catalytically driven nanorotors, *JACS Commun.* 129 (2007) 14870.
- [7] S. Sundararajan, P.E. Lammert, A.W. Zudans, V.H. Crespi, A. Sen, Catalytic motors for transport of colloidal cargo, *Nano Lett.* 8 (2008) 1271–1276.
- [8] G. Oster, Darwin's motor, *Nature* 417 (2002) 25.
- [9] R.D. Astumian, Making molecules into motors, *Sci. Am.* 285 (2001) 56–64.
- [10] M. Schliwa, *Molecular Motors*, Wiley-VCH, Weinheim, 2003.
- [11] E.M. Purcell, Life at low Reynolds number, *Am. J. Phys.* 45 (1977) 3–11.
- [12] W.R. Browne, B.L. Feringa, Making molecular machines work, *Nat. Nanotechnol.* 1 (2006) 25–35.
- [13] A. Einstein, *Investigation on the Theory of Brownian Movement*, Dover Publications, 1956.
- [14] R.P. Feynman, R.B. Leighton, M. Sands, *The Feynman Lectures on Physics*, vol. 46, Addison-Wesley, Reading, MA, 1963, p. 1.
- [15] P. Hanggi, F. Marchesoni, F. Nori, Brownian motors, *Ann. Phys.* 14 (2005) 51–70.
- [16] H. Linke, M.T. Downton, M.J. Zuckermann, Performance characteristics of Brownian motors, *CHAOS* 15 (2005) 026111–026122.
- [17] E. Altintas, K.F. Böhringer, H. Fujita, Micromachined linear Brownian motor: transportation of nanobeads by Brownian motion using 3-phase dielectrophoretic ratchet, *J. Appl. Phys.* 47 (2008) 8673–8677.
- [18] H. Morgan, N.G. Green, *AC Electrokinetics: Colloids and Nanoparticles*, RSP, Hertfordshire, UK, 2003, p. 139.
- [19] M. Washizu, S. Suzuki, O. Kurosawa, T. Nishizaka, T. Shinohara, Molecular dielectrophoresis of biopolymers, *IEEE Trans. Ind. Appl.* 30 (1994) 835–843.
- [20] A. Castellanos, A. Ramos, A. Gonzales, N.G. Green, H. Morgan, Electrohydrodynamics and dielectrophoresis in microsystems: scaling laws, *J. Phys. D: Appl. Phys.* 36 (2003) 2584–2597.
- [21] H.S. Nalwa (Ed.), *Encyclopedia of Nanoscience and Nanotechnology*, vol. 6, ASP, Valencia, CA, USA, 2004, pp. 623–641.
- [22] H.C. Berg, *Random Walks in Biology*, Expanded Edition, Princeton University Press, Princeton, USA, 1993, pp. 42–45.
- [23] G.S. Oehrlein, Y. Zhang, D. Vender, M. Haverlag, Fluorocarbon high-density plasmas. 1. Fluorocarbon film deposition and etching using CF₄ and CHF₃, *J. Vac. Sci. Technol. A* 12 (1994) 323–332.
- [24] H.F. Arata, Y. Rondelez, H. Noji, H. Fujita, Temperature alternation by an on-chip microheater to reveal enzymatic activity of β -Galactosidase at high temperatures, *Anal. Chem.* 77 (2005) 4810–4814.
- [25] SEM result revealed that the height of Si mold was around 1.5 μ m, although the height was adjusted for 1 μ m. This was believed to be caused by maintenance of STS before etching of silicon which could change the etching speed.
- [26] H. Makamba, J.H. Jim, K. Lim, N. Park, J.H. Hahn, Surface modification of poly(dimethylsiloxane) microchannels, *Electrophoresis* 24 (2003) 3607–3619.
- [27] E. Verneuil, A. Buguin, P. Silberzian, Permeation-induced flows: consequences for silicone-based microfluidics, *Europhys. Lett.* 68 (2004) 412–418.
- [28] Electrode spacing was measured 3.5 μ m in the fabricated LBM-4.

Biographies

Ersin Altıntaş received the B.S., M.S. and Ph.D. degrees from electrical and electronic engineering of Middle East Technical University, Ankara, Turkey, and electrical engineering of The University of Tokyo, Tokyo, Japan in 2002, 2005, and 2008, respectively. His Ph.D. thesis dealt with the manipulation of Brownian motion as a driving source at nanoscale and its ratcheting by dielectrophoresis. He was a member of Center for International Research on MicroMechatronics (CIRMM), Institute of Industrial Science (IIS), The University of Tokyo. Since graduation, he has been working in NEC Corporation, Nanoelectronics Research Laboratories, Tsukuba, Ibaraki, Japan. His research interests focus on Micro-Electro-Mechanical Systems, AC electrokinetics, and bio-chemical sensors.

Edin Sarajlic received the M.Sc. and Ph.D. degrees from the University of Twente, The Netherlands in May 2001 and 2005, respectively. His Ph.D. thesis dealt with electrostatic stepper micromotors for a probe-based data storage system. Since 2005, he has been working as a Research Fellow in the Center for International Research on MicroMechatronics (CIRMM), Institute of Industrial Science (IIS), The University of Tokyo, Japan. His research interests focus on Micro-Electro-Mechanical Systems, particularly on the development of microactuators and micromachining methods for their fabrication.

Karl F. Böhringer received his Dipl.-Inform. degree from the University of Karlsruhe, Germany in 1990 and his M.S. and Ph.D. degrees in computer science from Cornell University, Ithaca, NY in 1993 and 1997, respectively. He was a Visiting Scholar at Stanford University in 1994–1995 and a Postdoctoral Researcher at the University of California, Berkeley from 1996 to 1998. He joined the University of Washington in Seattle, WA in 1998, where he is Professor of Electrical Engineering. He also held visiting faculty positions at the Universities of Tohoku, Tokyo, Kyoto (Japan), and São Paulo (Brazil). His research interests include microelectromechanical systems (MEMS), manipulation and assembly from macro- to nanoscales, microfluidic systems for the life sciences, and microrobotics. He has created, among others, multi-batch self-assembling systems, massively parallel microactuator arrays, and a walking microrobot.

Hiroyuki Fujita received the B.S., M.S. and Ph.D. degrees in electrical engineering from the University of Tokyo, Tokyo, Japan in 1975, 1977 and 1980, respectively. Since 2000, he has been Director of the Center for International Research on MicroMechatronics, also, since 1993, he has been a Professor, an Associate Professor (1981–1993), and a Lecturer (1980–1981) with the Institute of Industrial Science, the University of Tokyo. He is currently engaged in the investigation of microelectromechanical systems fabricated by IC-based processes and applications to optics, and bio/nanotechnology. He is also interested in autonomous distributed microsystems made by MEMS technology.